Journal of
Synchrotron Radiation

ISSN 0909-0495

Received 8 August 2008
Accepted 6 January 2009

A fast energy-dispersive multi-element detector for X-ray absorption spectroscopy

Edmund Welter,* Karsten Hansen, Christian Reckleben and Inge Diehl

Deutsches Elektronen-Synchrotron, A Research Centre of the Helmholtz Association, Notkestrasse 85, D-22607 Hamburg, Germany. E-mail: edmund.welter@desy.de

In this paper results are presented from fluorescence-yield X-ray absorption fine-structure spectroscopy measurements with a new seven-cell silicon drift detector (SDD) module. The complete module, including an integrated circuit for the detector readout, was developed and realised at DESY utilizing a monolithic seven-cell SDD. The new detector module is optimized for applications like XAFS which require an energy resolution of ~250–300 eV (FWHM Mn $K\alpha$) at high count rates. Measurements during the commissioning phase proved the excellent performance for this type of application.

Keywords: silicon drift detector; energy-dispersive detectors; XAFS; X-ray fluorescence.

1. Introduction

Today, fluorescence detection is one of the most often used methods for the registration of X-ray absorption fine-structure (XAFS) spectra. Most of these experiments employ energy-dispersive solid-state detectors. Commercially available Si(Li) and high-purity germanium (HPGe) detectors are operated at liquid-nitrogen temperatures whereas silicon drift detectors (SDDs) can be used near room temperature.

Since the XAFS effect is small, the statistical noise must be smaller than 10^{-2}–10^{-3}. This requires the detection of 10^4–10^6 photons in the fluorescence line of interest if Poisson statistics apply. Single-element detectors cover only a small fraction of the total solid angle and handle only a limited number of photons per second without detector dead-time-related problems leading to serious distortions of the measured XAFS spectra. Therefore these detectors are usually used as arrays with several independent cells.

SDDs were first described in 1984 (Gatti & Rehak, 1984). They have p^+ contacts at the back and front sides of the high-resistivity n-type photon-absorbing substrate. Depletion is achieved *via* a small n^+ contact (anode) in the centre of the detector cell. The n^+ contact is positively biased with respect to the mentioned surrounding p^+ electrodes.

This design gives a number of advantageous properties for XAFS spectroscopy and other methods with similar experimental demands. Characteristic of SDDs is the small charge-collecting capacitance owing to the small readout anode. This results in the possibility of achieving high count rates between 0.1 and 1 MHz with an energy resolution which is sufficient for XAFS spectroscopy (Strüder & Lechner, 1998). Moreover, SDDs do not need cryogenic cooling to liquid-nitrogen temperature but work at, or just 10–20 K below, room temperature (Strüder *et al.*, 1999; Lechner *et al.*, 2001).

Most commercially available SDD systems use single detector chips with active areas between 10 mm^2 and 100 mm^2. This type of detector is easy to handle and it is possible to register the detector signal using conventional signal-processing electronics like pre-amplifiers and shaping amplifiers, peak-finding analogue-to-digital converters with single- or multi-channel analyzers or digital signal processors (DSPs). Moreover, single-cell detectors suffer less from deterioration of the peak-to-background ratio owing to charge splitting at cell borders. By using arrays of several single-cell detectors it is possible to cover a larger solid angle than with using only one detector cell. However, more elaborate multi-cell designs covering large fractions of the total solid angle with minimized dead regions between detector cells are only possible with monolithic multi-cell detectors (Foran *et al.*, 2007).

Recently, we finished the fabrication and testing of a small number of seven-cell SDD detector modules with a good cost *versus* performance trade-off (Hansen *et al.*, 2008*a*). Modules of this type or with shape-modified and/or larger SDD cells/arrays can be the basis for further complex arrangements of modules like one-dimensional, two-dimensional (Hansen *et al.*, 2008*a*) or 4π detectors (Hansen & Tröger, 2000).

2. Experimental

All experiments were performed at the bending-magnet beamline C at the Hamburger Synchrotronstrahlungslabor (HASYLAB) at DESY. For XAFS experiments the Si 111 double-crystal monochromator was detuned to 60% of the maximum intensity to suppress higher harmonics contamination of the monochromatic beam. The beam size on the sample was 8 × 1 mm. For count-rate-dependent measurements of fluorescence spectra the monochromator was detuned to values between 1% and 90% of the maximum intensity. The

Table 1
Overview of the samples used.

Sample	Composition	Supplier
As in Fe_2O_3	$Na_2HAsO_4{\cdot}7H_2O$, 1.9 mg; Fe_2O_3, 115.2 mg	Sigma-Aldrich, Hannover, Germany
Stainless steel	Fe/Cr18/Ni8/Mo3, 5 µm	Goodfellow, Huntingdon, UK
Mn foil	Mn, 5 µm	Goodfellow, Huntingdon, UK
Eu_2O_3	4.6 mg in 200 mg cellulose	Kristallhandel Kelpin, Heidelberg, Germany

slit size was left unaltered during these experiments to avoid artefacts owing to sample inhomogeneities. Unless stated otherwise, the distance between the detector and the sample was 7 cm. Detector and sample were in vacuum and the detector was operated windowless.

Table 1 gives an overview of the samples used. They were chosen to demonstrate the performance of the detector under working conditions for which a detector system consisting of several relatively small detector cells is advantageous.

2.1. Detectors

2.1.1. SDD detector. Fig. 1 shows one of our currently available SDD modules (Hansen *et al.*, 2008*a*). The insert shows the magnified sensor head containing the seven-cell SDD chip which was purchased from PNsensor (Munich, Germany) and a seven-channel readout integrated circuit (ROIC). The head housing is set up from precisely shaped parts made of AlN ceramics. This material was chosen because of its high electrical resistance and because it causes no X-ray fluorescence above ∼2 keV. The power dissipated in the sensor head can be removed by a thermoelectrical cooler into the long tube made of Cu for good heat transport. The module has a wrench size of 16 mm.

The SDD chip is a hexagonal arrangement of seven hexagonal cells with integrated junction-field effect transistors (JFET) in the centre of each cell. Each cell has an active area of 7 mm^2 and a thickness of 450 µm, enabling measurements with quantum efficiencies of >50% up to 17.5 keV (Hansen *et al.*, 2008*a*). The readout anode of the SDD is connected to the gate of the monolithically integrated JFET structure. That enables on-detector chip amplification resulting in an improved spectral resolution at higher count rates (Strüder & Soltau, 1995). The use of a specialized ROIC allows the readout of all detector cells in parallel and permits the set up of modules with small-form factors. A suitable data-acquisition (DAQ) system capable of processing the data of multi-element SDDs has been available at DESY for six years (Hansen *et al.*, 2002).

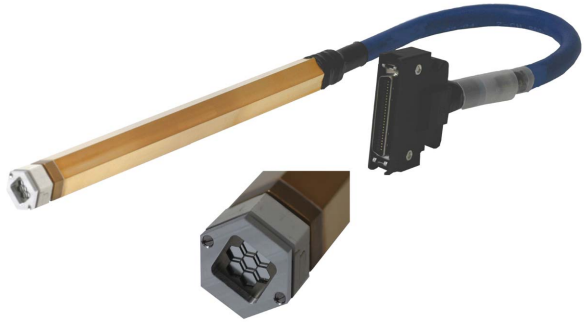

Figure 1
Photograph of a seven-cell SDD module.

The borders between the cells are covered by a 450 µm-thick Zr mask. This prevents absorption of photons in a ∼100 µm broad stripe at the cell borders and in a ∼300 µm-diameter region of the cell centre where the JFET is placed. Absorption of photons in these regions leads to a loss of charge carriers and degrades the detector peak-to-background ratio. Previous spatially resolved investigations of the spectral performance had shown that masking improves the peak-to-background ratio by a factor of up to ten depending on the working distance between the sample and detector (Kappen *et al.*, 2001; Welter & Hansen, 2007). Zr leaves a broad gap in the desired energy range of operation between its *L* and *K* X-ray emission lines. One of the currently available modules which was not used during this study is equipped with a 1.3-mm-thick Al_2O_3 ceramic mask.

The in-house designed ROIC (Diehl *et al.*, 2007) is bonded to the SDD chip. It is placed behind a radiation-protection shield to avoid radiation damage. The shield is a sandwich of 500 µm AlN (housing), 250 µm Ti and 500 µm Ta. This design not only protects the ROIC it also minimizes the backwards fluorescence onto the SDD chip which would otherwise produce artefacts in the measured spectra.

All seven cells are read out using DESY's 120-channel DAQ system and powered by an external supply developed within the framework of an earlier SDD R&D project. The data exchange between the beamline-control software and the DAQ system is carried out *via* an Ethernet-socket connection. This system will soon be replaced by a new DSP system based on the peripheral component interconnect extensions for instrumentation (PXI) architecture which is especially designed for the operation of our seven-cell SDD detector. Power supplies and temperature regulation of the detector will be incorporated into this new system.

In contrary to the second detector system used during this study, the SDD module shows not only a count-rate-dependent dead-time but also a count-rate-independent dead-time of 16.6% of the respective real count rate owing to the readout scheme using a sixfold multiplexer. The reason for this dead-time contribution is that each cell is read out once during one multiplexer cycle. During the readout the respective detector cell cannot register events (Hansen *et al.*, 2008*b*). In XAFS spectroscopy only the count-rate-dependent part of the dead-

time needs to be considered, because a constant dead-time does not damp the amplitude of the oscillations in the normalized XAFS spectra.

2.1.2. HPGe detector. The seven-cell HPGe detector (Canberra GL0110*7) is routinely used at HASYLAB's EXAFS beamlines for the registration of fluorescence-yield XAFS spectra. Each of its seven detector cells has an active area of 100 mm^2 and a thickness of 10 mm, and are placed 5 mm behind 25 µm-thick Be windows. The detector is operated at liquid-nitrogen temperature applying a bias voltage of −500 V.

In the standard set-up, which was also used during this study, the output of the seven transistor reset pre-amplifiers is fed into seven DSPs (Canberra 2060). The DSP peaking time was set to 1.2 µs and the flat top to 0.3 µs. Under these conditions the average spectral resolution is 200–250 eV (FWHM Mn $K\alpha$) and dead-time T = 2.96 µs. The dead-time was determined using the fast event-counting electronics of the DSPs (ICR) as a measure of the 'real' count rate. In standard EXAFS applications the detector is usually operated at count rates smaller than 50 kHz per cell to avoid spectrum distortions owing to saturation effects.

3. Results and discussion

3.1. Dead-time of the SDD modules

The dead-time was determined by measuring a series of Mn-fluorescence spectra at variable incoming intensities. The incoming intensity was changed by detuning of the second monochromator crystal, thus avoiding any changes of the size or position of the beam spot on the sample. The incoming beam had a photon energy of 6650 eV. Each spectrum was measured for 30 s; the incoming intensity was measured using a standard HASYLAB ionization chamber.

Since the SDD modules do not have separate fast event-counting electronics we estimated the incoming or 'real' count rate by extrapolating the increase of the processed count rate (R_p) using the ionization-chamber current measured at low count rates (<20 kcounts s^{-1}, first five data points in Fig. 2) to count rates of ∼350 kcounts s^{-1}. This can be done because the count rate loss owing to detector dead-time is negligible at small count rates. The 'real' count rate (R_0) was calculated by multiplying the extrapolated count rates by 6/5 to account for the fact that each detector cell is inactive for 1/6 of the time.

Finally we fit equation (1) to the measured values of R_p over R_0,

$$R_p = (5/6)R_0 \exp(-R_0 T). \quad (1)$$

The factor 5/6 in front of the well known formula for detectors with paralysable response function accounts for the mentioned count-rate-independent dead-time owing to the read-out scheme. The fit resulted in a value for T of 820 ns. This result is in good agreement with the dead-time which can be calculated from the values presented by Hansen *et al.* (2008*b*) (T = 750 ns), who used another sample and another detector module.

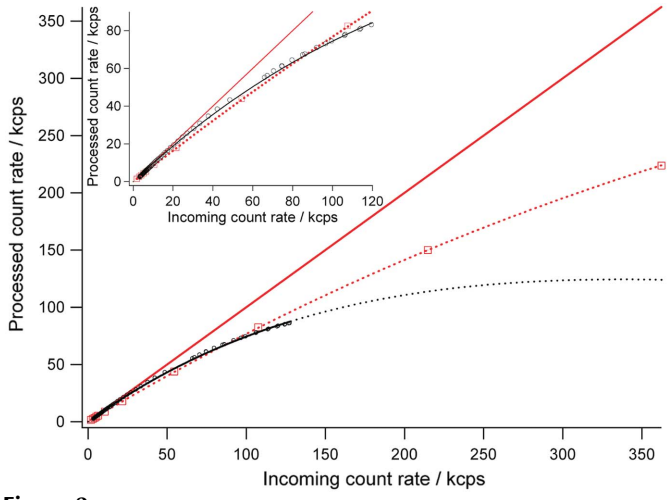

Figure 2
Throughput function of cell 2 of the seven-cell SDD module. Red squares: sum of all processed counts (R_p). Straight red line: incoming count rate (R_0). Dotted red line: fit to the function $R_p = 5/6{*}R_0 \exp(-R_0 T)$ with T = 0.82 µs being the peak processing time of the system. Shown in black are the respective values for one cell of the HPGe detector. The inset shows details of the curves at lower count rates.

Fig. 2 also shows plots of R_p and R_0 over R_0 for the SDD and for the HPGe detector. At count rates greater than 80 kcounts s^{-1} the HPGe detector shows smaller count rate losses owing to detector dead-time. This is caused by the constant 16.6% dead-time of the SDD detector modules. Above 80 kcounts s^{-1} the efficiency of the SDD modules becomes higher than the efficiency of our HPGe detector system.

3.2. As in Fe_2O_3

A sample with traces of As in Fe_2O_3 was chosen as an example of a sample containing a trace element in a matrix producing a large fluorescence background. It is furthermore of practical importance because Fe is used as an 'active barrier' material for the clean up of As-contaminated groundwater (Köber *et al.*, 2005*a*,*b*).

The ratio between the integral-count rate and the number of detected As $K\alpha$ photons was ∼60/1, not unusual for real samples even if filters are used in front of the detector. Fig. 3 shows an emission spectrum of this sample. This spectrum was measured for 10 s and used to set the region of interest for the integration of the As $K\alpha$ peak.

In order to prove that the precision of the count rate in a selected emission line is only determined by Poisson photon statistics, a dummy scan was performed. A total of 200 emission spectra were measured in a row without changing any parameter. The counting time for each spectrum was 5 s. The average integral-count rate per cell was of the order of 10000 counts s^{-1}; the average count rate within the As $K\alpha$ emission line was 166 counts s^{-1}. Fig. 4 shows the distribution of count rate values around the average value for cell 3. Table 2 lists the average count rate N for all cells, together with the expected standard deviation $\sigma_{exp} = N^{1/2}$, the measured stan-

Table 2
Statistical parameter derived from 200 consecutive fluorescence spectra.

N: number of counts expected (exp) and measured (meas). σ: standard deviation.

Cell number	2	3	4	5	6	7
Average *N*	895.3	820.0	861.5	798.6	855.5	782.7
σ_{exp}	29.9	28.6	29.4	28.3	29.2	28.0
σ_{meas}	29.7	29.3	30.4	28.3	29.5	29.9
Minimum *N*	807	739	788	717	785	684
Maximum *N*	974	913	948	878	958	856

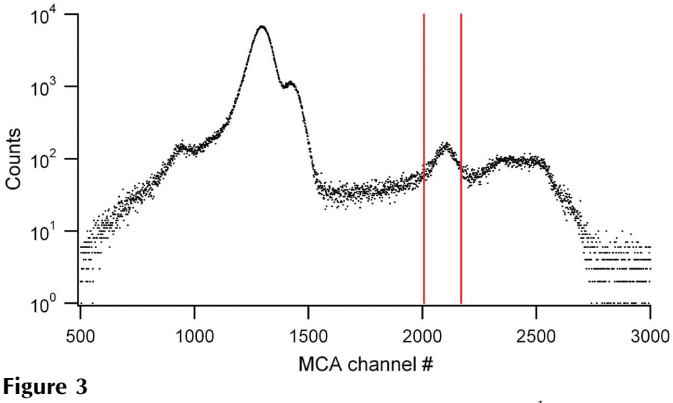

Figure 3
X-ray emission spectrum of a sample containing 4 mg g^{-1} As in Fe_2O_3. The vertical lines mark the borders for the integration of the As $K\alpha$ count rate for fluorescence-yield XAFS.

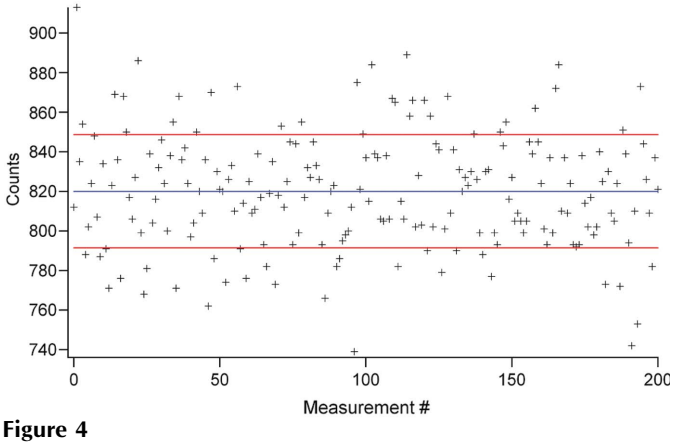

Figure 4
Number of As $K\alpha$ photons detected in cell 3 of the SDD module. Incoming beam energy: 11950 eV. Count rates are corrected for decreasing storage-ring current. Blue line: average value (*N*). Red lines: $N \pm N^{1/2}$.

dard deviation σ_{meas} and the maximum and minimum count rate. The observed agreement between σ_{exp} and σ_{meas} clearly proves the absence of any systematic errors in the count rates measured by the detector system.

Fluorescence-yield XAFS (fl-XAFS) spectra of this sample were also measured. Fig. 5 shows normalized As *K*-edge X-ray absorption near-edge spectra (XANES) measured with the SDD module and for comparison with the seven-cell HPGe detector. Background correction and normalization of the edge jump were carried out following standard procedures for XAFS spectrum evaluation. The average absolute number of As $K\alpha$ photons detected at energies above 11890 eV in the

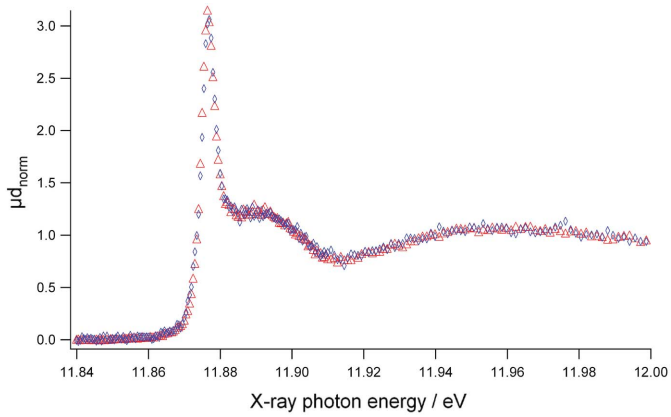

Figure 5
Normalized As *K*-edge fluorescence-yield XANES spectra of the As-in-Fe_2O_3 sample, detected with the SDD (blue, diamonds) and for comparison with an HPGe detector (red, triangles) at almost equal count rates.

SDD and HPGe detector fl-XAFS spectra is ~2200 and 2800 counts per point, respectively. Under these conditions both detectors yield similar fl-XAFS spectra.

3.3. Ni *K*-edge XAFS in $FeCr_{18}Ni_{10}Mo_3$

$FeCr_{18}Ni_{10}Mo_3$ is another example of a sample producing a high background-count rate. Thus far it is comparable with the As-in-Fe_2O_3 sample. The difference with the latter sample is the fact that the separation between the emission lines of the matrix elements (Cr, Fe) and the emission line of interest (Ni $K\alpha$) is much smaller, ~1000 eV compared with ~4000 keV.

The Ni content and the thickness of the foil (5 μm) were suited for the simultaneous registration of the transmission and of the fl-XAFS spectra. Fig. 6 displays the EXAFS spectra measured in both modes. The fl-EXAFS spectrum is the sum of the counts in all seven SDD cells. We measured the EXAFS spectrum with equidistant steps in *k* space with a step size of ~0.04 Å^{-1}. The measuring time per point was constant below the edge (2 s) and multiplied by k/k_0 (with k_0 being the *k* value at the start of this scan region) above the edge, *i.e.* the time per

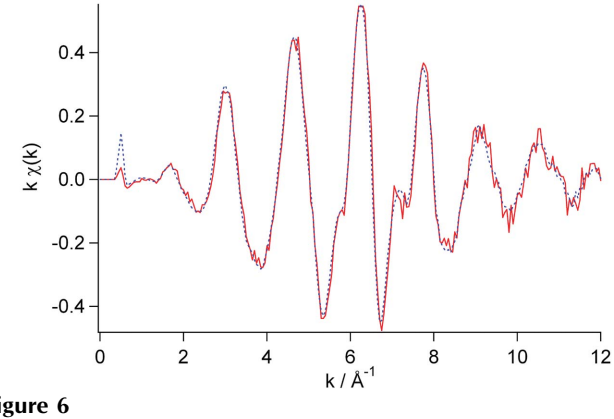

Figure 6
Ni *K*-edge EXAFS spectra measured on a stainless steel foil in transmission (dotted blue) and SDD-detected fluorescence (solid red) mode XAFS. The fl-EXAFS spectrum is not corrected for damping owing to self-absorption or detector dead-time.

point was 2 s × k/k_0. The accumulated average number of counts in the Ni $K\alpha$ line is 54000 representing a count rate of ∼3.9 kHz per cell. The integral-count rate, *i.e.* the sum of all counts within the measurement-time interval, was of the order of 60 kHz per cell (sum-count rate of the seven used detector cells, 420 kHz). Apart from the slightly higher noise level of the fl-EXAFS spectrum, no deviation between the two spectra is visible. Although the count rate normalized to the active area is 8.6 kcounts s^{-1} mm^{-2}, corresponding to a count rate of 430 kHz in a single-cell detector with an active area of 50 mm^2, the EXAFS spectrum in Fig. 6 shows no signs of damping owing to dead-time loss of counts.

3.4. White line of Eu_2O_3

Like many other lanthanide oxides the Eu_2O_3 L_3-edge absorption spectrum shows a very strong 'white line', an intense peak directly above the absorption edge. Here, the fluorescence-count rate changes by several orders of magnitude in a narrow region of the spectrum and reaches high absolute values on top of the peak. In Fig. 7 we show four normalized XANES spectra of the Eu oxide sample. Two of these spectra were measured with the SDD at different count rates (Table 3), the third with the seven-cell HPGe detector and finally the fourth in transmission mode.

The three fl-XANES spectra are corrected for damping owing to self-absorption using the XANES algorithm from the *Athena* XAFS data-treatment code (Ravel & Newville, 2005). A comparison of the three normalized fl-XANES spectra with the transmission-XANES spectrum shows a significant damping of the white-line intensity for the HPGe detector and to a lesser degree for the SDD operated at the higher count rate. With the SDD operated at lower count rate no damping can be observed. These differences are caused by dead-time counting-loss effects of the detector systems.

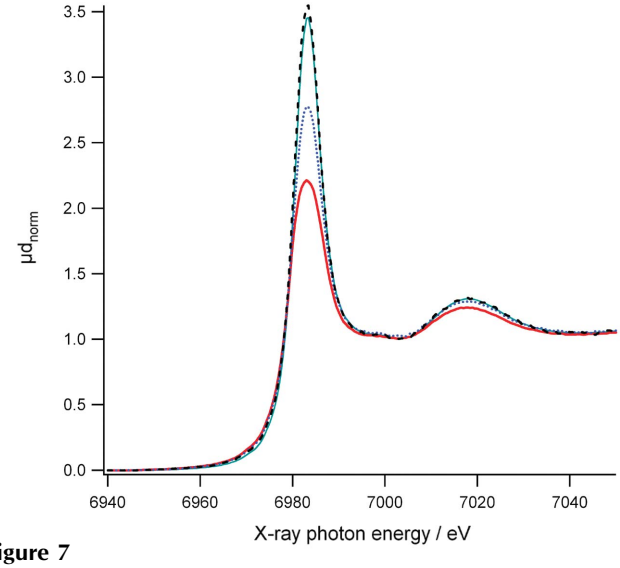

Figure 7
Eu L_3 XANES spectra of a Eu_2O_3 sample. The four spectra are detected using transmission (green, solid line), the SDD at a low count rate (black, dashed line), the SDD at a high count rate (blue, dotted line) and with a HPGe detector (red, lower solid line). All fl-XAFS spectra are corrected for damping owing to self absorption.

Table 3
Registered count rates.

Energy (eV)	Counts s^{-1} $cell^{-1}$	Counts s^{-1} mm^{-2}
SDD (low count rate)		
6900	1556	222
6983	32637	4662
7200	15903	2272
SDD (high count rate)		
6900	6352	907
6983	117458	16780
7200	61280	8754
HPGe		
6900	2948	29
6983	83713	837
7200	50753	508

By knowing the dead-time of a detector system it is possible to correct the damping effect caused by it (Ciatto *et al.*, 2004). In EXAFS spectroscopy applications, however, even the most careful dead-time correction solves only one part of the problem, the damping of the EXAFS amplitude. The important statistical quality of the data is determined by the number of actually detected photons and a proper measurement of the small (10^{-2}–10^{-3}) EXAFS effect makes excellent statistical data quality necessary. Correction of the damping can obviously not improve the statistical quality of the data.

The integral-active area of a seven-cell SDD module is 49 mm^2, which is about half the size of one of the seven HPGe cells. The advantage of distributing the incoming photons over seven independent cells is clearly discernible in Fig. 7. The damping of the white line owing to the detector dead-time is much smaller than in the spectrum from the larger HPGe detector although the count rate per mm^2 of active detector area is a factor of 4 and 16 higher for the low-count-rate and high-count-rate SDDs, respectively (see Table 3). Because of the more effective covering of the total solid angle with less spectroscopically inactive areas between, the monolithic multi-cell detectors employ this advantage more effectively than arrays of single-cell detectors with discrete readout electronics as presented in the literature earlier (Goulon *et al.*, 2005).

4. Conclusion

We have performed fl-XAFS test measurements with a new SDD system based on monolithic seven-cell SDD chips and integrated readout electronics. The samples for these test measurements were chosen to yield high integral count rates. The results were compared with results yielded from a germanium detector system routinely used for fl-XAFS experiments at HASYLAB. Because of its significantly shorter detector-system dead-time the SDD system proved to be very useful for applications where a high integral count rate is necessary. Using the SDD modules it is possible to reach very high count rates per mm^2 of active area compared with energy-dispersive solid-state detectors with large planar pn diodes. The energy resolution of 250–300 eV which can be

achieved at temperatures at or just below room temperature is sufficient for most XAFS applications.

While the modules presented are already a useful working detector system it is easily possible to use components which were developed in the framework of our project to assemble larger SDD arrays made up from SDD chips with different form factors.

The authors would like to thank H. Klär, A. Venzmer, E. Wüstenhagen, A. Titze, D. Hammer and W. O. Lange from DESY-FEC for their active help during the tests of the module.

References

Ciatto, G., d'Acapito, F., Boscherini, F. & Mobilio, S. (2004). *J. Synchrotron Rad.* **11**, 278–283.

Diehl, I., Hansen, K. & Reckleben, C. (2007). *Prcoeedings of the 33rd European Solid-State Circuits Conference (ESSCIRC 2007)*, 11–13 September 2007, Munich, Germany, pp. 296–299.

Foran, G., Hester, J., Garrett, R., Dressler, P., Fonne, C., Beau, J.-O. & Lampert, M.-O. (2007). *Proceedings of the 13th International Conference on X-ray Absorption Fine Structure (XAFS13)*, 9–14 July 2006, Stanford, CA, USA, edited by B. Hedman and P. Pianetta. Melville: AIP Press.

Gatti, E. & Rehak, P. (1984). *Nucl. Instrum. Methods Phys. Res.* **225**, 608–614.

Goulon, J., Rogalev, A., Goujon, G., Gauthier, C., Moguiline, E., Solé, A., Feite, S., Wilhelm, F., Jaouen, N., Goulon-Ginet, C., Dressler, P., Rohr, P., Lampert, M.-O. & Henck, R. (2005). *J. Synchrotron Rad.* **12**, 57–69.

Hansen, K., Reckleben, C., Diehl, I. & Klär, H. (2008*b*). *Nucl. Instrum. Methods Phys. Res. A*, **589**, 250–258.

Hansen, K., Reckleben, C., Diehl, I. & Welter, E. (2008*a*). *Nucl. Instrum. Methods Phys. Res. A*, **585**, 76–82.

Hansen, K., Reinecke, M., Klär, H. & Benca, M. (2002). *IEEE Trans. Nucl. Sci.* **49**, 541–547.

Hansen, K. & Tröger, L. (2000). *IEEE Trans. Nucl. Sci.* **47**, 2748–2757.

Kappen, P., Tröger, L., Hansen, K., Reckleben, Ch., Lechner, P., Strüder, L. & Materlik, G. (2001). *Nucl. Instrum. Methods Phys. Res. A*, **467–468**, 1163–1166.

Köber, R., Daus, B., Ebert, M., Mattusch, J., Welter, E. & Dahmke, A. (2005*a*). *Environ. Sci. Technol.* **39**, 7650–7655.

Köber, R., Welter, E., Ebert, M. & Dahmke, A. (2005*b*). *Environ. Sci. Technol.* **39**, 8038–8044.

Lechner, P., Fiorini, C., Hartmann, R., Kemmer, J., Krause, N., Leutenegger, P., Longoni, A., Soltau, H., Stötter, D., Strüder, L. & Weber, U. (2001). *Nucl. Instrum. Methods Phys. Res. A*, **458**, 281–287.

Ravel, B. & Newville, M. (2005). *J. Synchrotron Rad.* **12**, 537–541.

Strüder, L. & Lechner, P. (1998). *Naturwissenschaften*, **85**, 539–543.

Strüder, L., Meidinger, N., Stotter, D., Kemmer, J., Lechner, P., Leutenegger, P., Soltau, H., Eggert, F., Rohde, M. & Schulein, T. (1999). *Microsc. Microanal.* **4**, 622–631.

Strüder, L. & Soltau, H. (1995). *Radiat. Protect. Dosim.* **61**, 39–46.

Welter, E. & Hansen, K. (2007). *Proceedings of the 13th International Conference on X-ray Absorption Fine Structure (XAFS13)*, 9–14 July 2006, Stanford, CA, USA, edited by B. Hedman and P. Pianetta. Melville: AIP Press.